Catalytic Action of Fuculose 1-Phosphate Aldolase (Class II) As Derived from Structure-Directed Mutagenesis[†,‡]

Andreas C. Joerger,[§] Claudius Gosse,[||] Wolf-Dieter Fessner,[||] and Georg E. Schulz*[,§]

Institut für Organische Chemie und Biochemie, Albert-Ludwigs-Universität, D-79104 Freiburg im Breisgau, Germany, and Institut für Organische Chemie, Technische Universität, D-64287 Darmstadt, Germany

Received December 2, 1999; Revised Manuscript Received February 28, 2000

ABSTRACT: Previous analyses established the structures of unligated L-fuculose 1-phosphate aldolase and of the enzyme ligated with an inhibitor mimicking the substrate dihydroxyacetone phosphate. These data allowed us to suggest a catalytic mechanism. On the basis of this proposal, numerous mutations were now introduced at the active center and tested with respect to their catalytic rates and their product distributions. For several mutants, the structures were determined. The results demonstrate the catalytic importance of some particular residues in defined conformations and in the mobile C-terminal chain end. Moreover, they led to a modification of the proposed mechanism. The effect of some mutations on enantioselectivity and on the ratio of diastereomer formation indicates clearly the binding site of the aldehyde moiety in relation to the other substrate dihydroxyacetone phosphate.

L-Fuculose 1-phosphate aldolase (FucA,[1] EC 4.1.2.17) from *Escherichia coli* catalyzes the reversible cleavage of L-fuculose 1-phosphate (Fuc1P) to dihydroxyacetone phosphate (DHAP) and L-lactaldehyde (Figure 1), which is a central step in the bacterial L-fucose metabolism (*1*). There is an increasing interest in FucA (*2, 3*) and functionally related aldolases because they are catalysts for stereospecific carbon−carbon bond formation (*4*−*7*). In particular, these aldolases open an alternative approach for the synthesis of rare sugars and related chiral compounds that are often difficult to prepare by conventional organic synthesis. It has been shown that all DHAP-dependent aldolases studied so far possess a high specificity for the DHAP nucleophile, but accept a great variety of different aldehyde electrophiles (*6, 8, 9*).

Aldolases have been subdivided into two classes according to their reaction mechanisms. Class I aldolases are characterized by a covalent intermediate, which is a protonated Schiff base formed between an essential lysine residue and the carbonyl carbon of the substrate (*10*−*13*). Structures of class I aldolases have been reported for fructose 1,6-bisphosphate aldolase from rabbit muscle (*14, 15*), human muscle (*16, 17*), *Drosophila melanogaster* (*18*), and *Plasmodium falciparum* (*19*) as well as for other aldolases such as 2-keto-3-deoxy-6-phosphogluconate aldolase from *Pseudomonas putida* (*20*), *N*-acetylneuraminate aldolase from *E. coli* (*21, 22*), and 7,8-dihydroneopterin aldolase from *Staphylococcus aureus* (*23*).

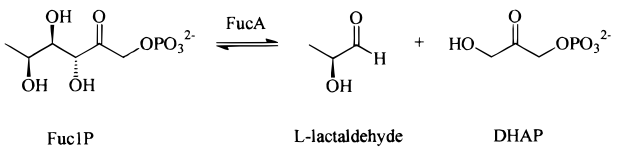

FIGURE 1: Reaction catalyzed by L-fuculose 1-phosphate aldolase (reversible aldol cleavage and addition).

In contrast, the active center of a class II aldolase contains a metal ion (usually zinc) stabilizing the reaction intermediates. FucA was the first structurally established class II enzyme (*24*−*26*). Meanwhile, two other class II aldolases structures have been determined, namely, those of fructose 1,6-bisphosphate aldolase (*27*−*29*) and of L-rhamnulose 1-phosphate aldolase (M. Krömer and G. E. Schulz, personal communication), both from *E. coli*.

The analyzed enzyme FucA is a homotetramer of 215 amino acid residues with one zinc ion per subunit and a rare C_4 symmetry. The structure had been initially determined in a tetragonal space group with crystals grown from ammonium sulfate. The chain fold is quite distinct from the $(\beta\alpha)_8$-barrels of the structurally established class I aldolases. The active centers are located at the four subunit interfaces of the C_4 tetramer with residues from two adjacent subunits contributing to each of them.

Following enzymological studies with Fuc1P analogues and phosphoglycolohydroxamate (PGH) as a transition state analogue of the DHAP moiety (*30*), FucA crystals were soaked with PGH. The complex of FucA and PGH could be

[†] The project was supported by BMBF Grants BEO-0310745 and BEO-0310748.

[‡] The coordinates and structure factors are deposited with the Protein Data Bank under accession codes 1DZU, 1DZV, 1DZW, 1DZX, 1DZY, and 1DZZ.

* To whom correspondence should be addressed: Institut für Organische Chemie und Biochemie, Albertstrasse 21, D-79104 Freiburg im Breisgau, Germany. Phone: +49-761-203-6058. Fax: +49-761-203-6161. E-mail: schulz@bio.chemie.uni-freiburg.de.

[§] Albert-Ludwigs-Universität.

[||] Technische Universität.

[1] Abbreviations: Del(207−215) and Del(211−215), mutants in which the denoted chain segments have been deleted (positions inclusive); DHAP, dihydroxyacetone phosphate; FucA, L-fuculose 1-phosphate aldolase; Fuc1P, L-fuculose 1-phosphate; PGH, phosphoglycolohydroxamate; Tyr113′, all primes refer to a particular active center defined by the zinc ion and denote residues contributed from a neighboring subunit.

10.1021/bi9927686 CCC: $19.00
Published on Web 04/26/2000

analyzed in a cubic crystal form (*26*). The ligand PGH exhibited the binding mode of the substrate DHAP and allowed us to suggest a mechanism for the catalysis (*26*, *30*) that is likely to apply also for L-ribulose 5-phosphate 4-epimerase (*31*). On the basis of this suggestion, we introduced several mutations in the active center of FucA for further elucidation of the mechanism and of the role of the flexible C-terminal tail (residues 207−215), which cannot be detected in the X-ray structure.

MATERIALS AND METHODS

Mutagenesis. For mutagenesis, we took the expression plasmid pKKFA2 (*25*), excised the gene with *Eco*RI and *Pst*I, and cloned it into bacteriophage vector M13mp19 (Boehringer-Mannheim). The Kunkel method (*32*) was used to create mutants R212A, E214A, and E215A. All other mutations were created with the phosphorothioate method (*33*) using a kit from Amersham. DNA was sequenced with a direct blotter (GATC-1500) using the BioCycle Sequencing Kit (GATC) with Thermo Sequenase from Amersham.

Protein Production and Purification. Each mutated gene was cloned into the expression vector, yielding a pKKFA2 homologue, which was then transformed into *E. coli* strain JM105. For protein production, the cells were grown in 1.2 L of Luria-Bertani/ampicillin broth (LBA) up to an optical density of 0.6 at 578 nm and then induced by adding isopropyl β-thiogalactopyranoside (IPTG) to a final concentration of 0.5 mM. After an additional 8−11 h, the cells were harvested, yielding between 5 and 7 g of wet bacteria containing 200−600 mg of FucA. The cells were disrupted by sonication for 10 min, and DNA was precipitated with Polymin P. The same two-step purification procedure that was used for the wild type was applied (*25*), including anion-exchange chromatography (DEAE-Sepharose CL-6B) and subsequent gel permeation chromatography. The high expression level allowed us to restrict ourselves to the most active fractions, resulting in 40−150 mg of crystallizable protein. All steps were carried out in 20 mM Tris-HCl buffer (pH 7.6) with 1 mM $ZnCl_2$ and 10 mM 2-mercaptoethanol. Protein concentrations were determined photometrically using calculated extinction coefficients, i.e., $\epsilon_{280} = 20\,380$ M^{-1} cm^{-1} for wild-type FucA (*34*).

Crystallization and Structure Analysis. The crystallization of FucA mutants followed the procedure described for the wild type (*35*). Crystals grew usually within 2 weeks to maximum sizes of about 700 μm × 300 μm × 300 μm. They belonged to the tetragonal space group $P42_12$ and were isomorphous with the wild-type crystals ($a_{tet} = b_{tet} = 93.7$ Å, $c_{tet} = 42.8$ Å). All cell parameters agreed within 1.2%. Data were collected at room temperature on a rotating anode X-ray generator with an area detector (model RU200B, Rigaku, or model X1000, Siemens) and processed with the program XDS (*36*). After a first round of rigid body refinement with the program X-PLOR (*37*), difference Fourier maps were used to apply the appropriate changes at the respective models. The models were further refined using the program REFMAC (*38*). Water molecules were automatically introduced, removed, and refined using a procedure that alternates between the programs REFMAC and ARP (*39*). The stereofigures were produced with the programs O (*40*), MOLSCRIPT (*41*), and Raster3D (*42*).

Activity Measurements. The catalytic activity for the cleavage of Fuc1P was determined with a coupled continuous assay (*43*). In the first step, Fuc1P is cleaved to L-lactaldehyde and DHAP. As second step, DHAP was reduced using rabbit muscle glycerol 3-phosphate dehydrogenase (Boehringer-Mannheim or Fluka) and NADH, the consumption of which was monitored photometrically at 366 nm (Eppendorf, with filter). In the assay, 500 μL of buffer A [60 mM Tris, 60 mM KCl, 0.2 mM NADH, and 2.4 mM Fuc1P (pH 7.5)] was incubated for 10 min at 37 °C. After the addition of 2 units of glycerol 3-phosphate dehydrogenase, the reaction was started by adding the appropriate amount of the FucA mutant. The k_{cat} and K_M values were determined by measuring the activities at 7−12 substrate concentrations (three measurements each) usually in the range of 0.1−10 × K_M (maximum of 70 mM Fuc1P) and averaging the analyses by using Lineweaver−Burk, Hanes−Woolf, and Eadie−Hofstee methods. Using FucA, Fuc1P was synthesized enzymatically from *rac*-lactaldehyde and DHAP (*44*). DHAP was prepared from glycerol 3-phosphate using the respective oxidase (*45*).

Kinetic Enantioselectivity. *rac*-Lactaldehyde dimethylacetal (6.0 g, 50 mmol) in 50 mL of water was hydrolyzed by treatment with cation-exchange resin (Dowex AG50W-X8, H^+ form) at 60 °C and pH 6.8 for 8 h. After filtration, an aqueous solution of DHAP (10 mL, 10 mmol) was added and the mixture was adjusted to pH 6.8. Samples of 6 mL were incubated with 1 unit of the respective FucA mutant (control with wild-type FucA) at room temperature until the conversion of DHAP was about 90% complete as monitored by thin-layer chromatography (6/3/2 2-propanol/ammonia/water). After the addition of charcoal, the reaction mixture was stirred for 15 min and then filtered through a pad of silica gel before being concentrated under vacuum. The residue was dissolved in D_2O and analyzed by ^1H NMR spectroscopy (300 MHz). The product ratio was determined from the spectra by integrating the well-separated signals of the 1-H protons of the α-anomer of Fuc1P (3.95 ppm, dd; 3,4-D-*erythro* product from L-lactaldehyde) and the 4-H protons of the α-anomer of 6-deoxy-D-psicose 1-phosphate (3.89 ppm, t; 3,4-D-*erythro* product from D-lactaldehyde), taking into account the respective equilibrium ratios of α to β anomers as available from reference spectra (*3*).

Diastereoselectivity. The three compounds acetaldehyde, propionaldehyde, and isobutyraldehyde were incubated with DHAP under kinetically controlled conditions. For this purpose, an aqueous DHAP solution (10 mL, 10 mmol) was added to an aqueous aldehyde solution (20 mL, 20 mmol), and the pH was adjusted to 6.8. Samples (3 mL) were incubated with about 1 unit of the respective FucA mutant at room temperature (control with wild-type FucA) until the conversion of DHAP was about 90% complete as monitored by thin-layer chromatography (6/3/2 2-propanol/ammonia/water). The workup was carried out as described above, and the product analysis was performed by ^1H NMR spectroscopy (300 MHz, D_2O). The D-*erythro*/L-*threo* ratios (see below in Figure 7) were determined using the integration for the 4-H protons of the acetaldehyde adducts (L-*threo*, 4.32 ppm, dq; D-*erythro*, 4.20 ppm, dq), the 3-H protons of the propionaldehyde adducts (L-*threo*, 4.50 ppm, d; D-*erythro*, 4.43 ppm, d), and the methyl doublets for the isobutyraldehyde adducts (L-*threo*, 1.01 ppm; D-*erythro*, 0.93 ppm).

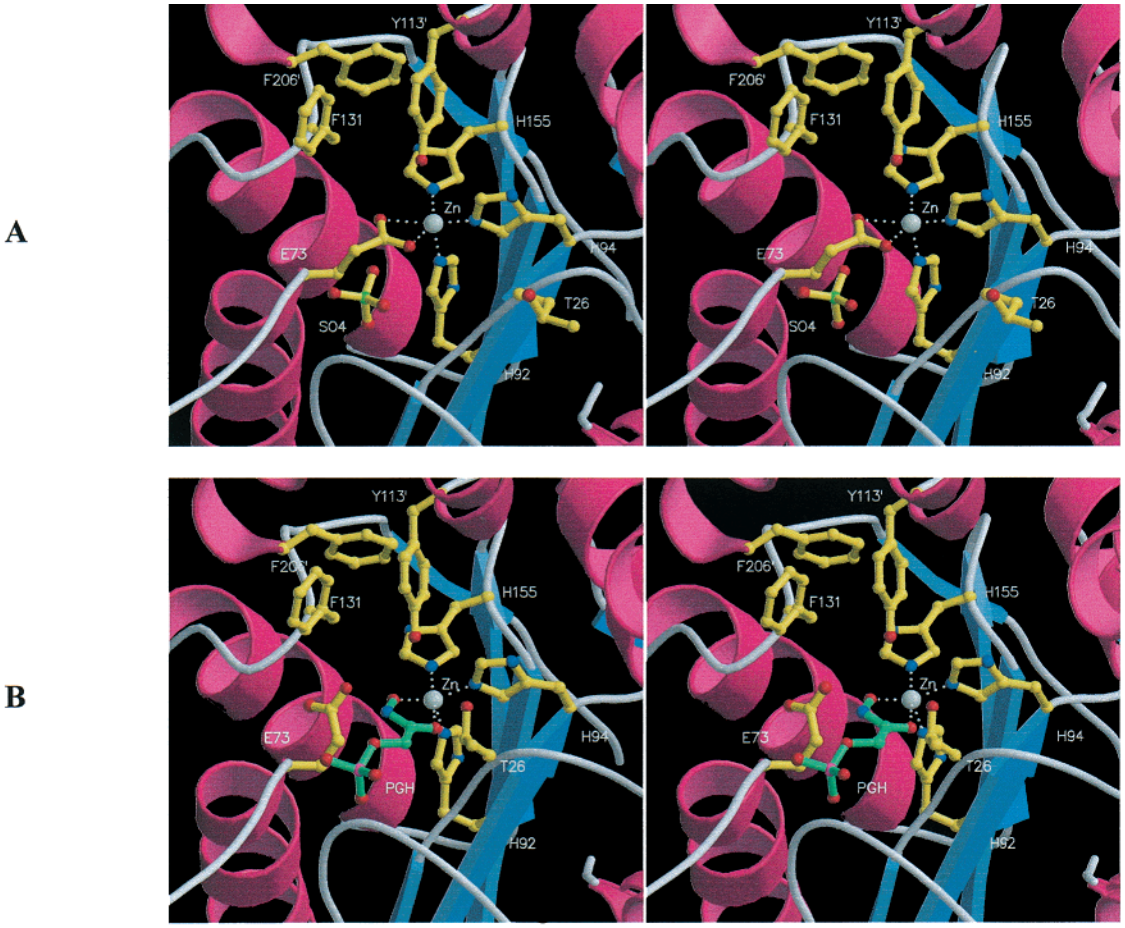

FIGURE 2: Stereoviews of the active center of wild-type FucA showing (A) the unligated state (*24*, *25*) and (B) the complex with the transition state analogue phosphoglycolohydroxamate (*26*).

RESULTS AND DISCUSSION

In the structure of the unligated enzyme (Figure 2A), the catalytic Zn^{2+} is coordinated by three histidines and the bidentate carboxylate group of Glu73 (*24*). Tyr113′ from the adjacent subunit with its hydroxyl group close to the Zn^{2+} (Zn−O distance of 3.5 Å) participates also in the formation of the active center. At one side, the active center is shielded by a nonpolar wall formed by the side chains of Tyr113′, Phe131, and Phe206′, where Phe206′ is the last conformationally defined residue at the C-terminal end of the polypeptide. The mobile tail of residues 207′−215′ is close enough to the active center to play a role in catalysis. Furthermore, the structure contained a SO_4^{2-} ion from the crystallization buffer trapped 7.4 Å away from the Zn^{2+}.

The inhibitor PGH was bound with its hydroxamate moiety at the Zn^{2+} displacing the bound carboxylate of Glu73 (Figure 2B). The phosphate moiety of PGH occupied the SO_4^{2-} position of the unligated structure. Furthermore, loop-(23−27) was rearranged and immobilized (lower *B*-factors); the largest movement was 3.5 Å for Thr26 Oγ.

A comparison of the unligated and the PGH-ligated structures suggested a reaction mechanism, which is sketched in the direction of the aldol addition in Figure 3. As the initial step, Glu73 deprotonates the C-3 atom of DHAP, producing an ene-diolate that is stabilized by Zn^{2+} complexation. This step was confirmed by a pK_a determination for a model compound mimicking DHAP complexed to Zn^{2+}, which showed that Zn^{2+} binding decreases the respective pK_a from

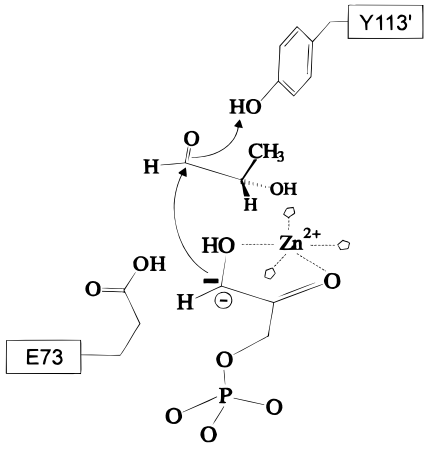

FIGURE 3: Catalytic mechanism of carbon−carbon bond formation by FucA as suggested previously (*26*, *30*). We now modify this proposal by assuming that Glu73, and not Tyr113′ with a decreased pK_a value, is the general acid because we observe appreciable activity with mutant Y113F.

19 to 8.4 (*46*). After nucleophilic attack at the carbon *Si* face of the aldehyde and subsequent C−C bond formation, the oxygen protonation was suggested to be mediated by Tyr113′ (*26*, *30*). To analyze the mechanism in further detail, numerous mutants were constructed to study the catalytic roles of residues 73 and 113′, of the mobile C-terminal tail (Figure 4), of the flexible loop(23−27), and of the nonpolar wall around Phe131.

Table 1: X-ray Data Collection Statistics of FucA Mutant Crystals[a]

	T26A	Y113F	Y113F/Y209F	F131A	R212A	E214A
resolution range (Å)	10−2.09	10−1.92	10−1.86	10−2.17	10−2.18	10−2.44
last shell (Å)	2.16−2.09	1.96−1.92	1.92−1.86	2.24−2.17	2.24−2.18	2.52−2.44
no. of unique reflections	10121 (822)	13096 (503)	15037 (1037)	10014 (840)	9269 (463)	6829 (568)
redundancy	3.1 (2.3)	4.7 (1.7)	4.9 (2.0)	3.2 (1.8)	3.9 (1.9)	4.1 (2.3)
R_{sym}[b] (%)	6.6 (15)	4.3 (18)	6.4 (17)	6.3 (13)	3.4 (17)	8.7 (21)
average I/σ_I	8.6 (4.8)	—[c]	8.5 (4.4)	10.1 (5.4)	—[c]	8.2 (3.3)
completeness (%)	87 (78)	87 (63)	91 (69)	95 (87)	89 (65)	92 (85)

[a] All values in parentheses refer to the last shell. [b] $R_{sym} = \Sigma_{hkl,i}|I_{hkl,i} - \langle I_{hkl}\rangle|/\Sigma_{hkl,i}I_{hkl,i}$. [c] Scaling done with the program MERGE (B. Dijkstra, Groningen, The Netherlands).

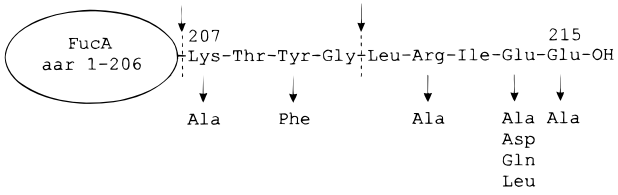

FIGURE 4: Amino acid sequence of the C-terminal tail of FucA, which is mobile and could not be detected in the X-ray structures (Table 2). The produced and analyzed mutations are denoted by arrows, including the truncation sites of the two C-terminal deletion mutants.

All mutants were sequenced at the DNA level, showing a mutation efficiency of around 90% for the mutants generated with the Eckstein method (*33*) and of about 50% for those created with the Kunkel method (*32*). The expression levels of all mutants were sufficient. The purification procedures followed that for the wild-type enzyme. A low solubility was observed for mutant E215A. Most of the mutants could be crystallized, always at conditions very similar to those of the wild type. Several mutants yielded crystals that were suitable for X-ray analysis. All of them were isomorphous to those of wild-type FucA, indicating that the mutations caused merely small structural changes.

X-ray Structure Analyses of FucA Mutants. Data were collected for six crystals of FucA mutants; they extended to resolutions between 1.9 and 2.4 Å (Table 1). First, the complete wild-type FucA model was adjusted to the observed structure factors $F_{obs,mut}$ by rigid body refinement. Subsequently, the ($F_{obs,mut}-F_{calc,wildtype}$) difference map was inspected. Usually, it contained only a few regions with density. These were interpreted, and the model was modified accordingly and refined to convergence (Table 2).

Table 2: Refinement Statistics for FucA Mutants[a]

	T26A	Y113F	Y113F/ Y209F	F131A	R212A	E214A
resolution (Å)	10−2.09	10−1.92	10−1.86	10−2.17	10−2.18	10−2.44
R_{cryst} (%)	15.0	15.9	16.8	15.2	14.4	14.9
R_{free}[b] (%)	20.7	20.7	21.6	21.8	20.0	22.6
no. of atoms						
polypeptide	1623	1612	1596	1591	1613	1597
zinc	1	1	1	1	1	1
sulfate	10	10	5	10	10	10
water	109	108	110	101	99	101
average *B*-factors (Å^2)						
polypeptide	18	27	26	25	25	17
zinc	11	22	21	17	17	13
sulfate	26	50	40	42	48	24
water	32	42	40	37	36	28
rmsd for C_α atoms[c] (Å)	0.14	0.36	0.37	0.16	0.33	0.17
last residue[d]	209	208	206	206	208	206
displaced residues[e]	—	24−26	24−26	—	25−26	—

[a] All root-mean-square deviations (rmsd) for bond lengths and bond angles were in the ranges 0.008−0.011 Å and 1.8−2.4°, respectively. [b] The size of the test set was 6%. [c] The deviations are between the respective mutant and wild-type FucA. [d] The C-terminal residue with a defined conformation. [e] Residues with C_α atoms displaced by more than 1 Å.

With none of the mutants did we observe an immobilization of the complete C-terminal tail. Yet, in some structures the electron density allowed us to extend the chain beyond Phe206′. In mutant T26A, the C-terminal helix could be extended up to Tyr209′ and in mutants Y113F and R212A up to Thr208′ (Figure 5). The conformation of the three additional residues in the structure of mutant T26A is the same as in a structure of the wild-type enzyme after

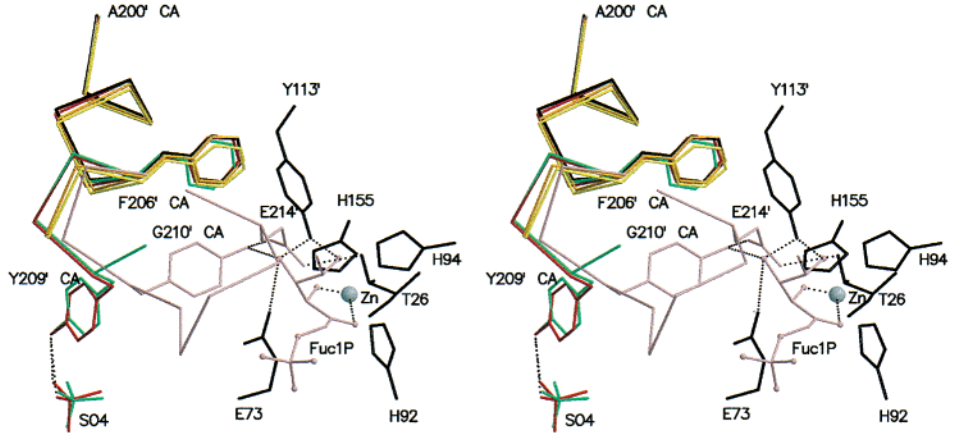

FIGURE 5: Superposition of the C-terminal ends of the conformationally defined polypeptide in wild-type FucA (black) (*24*, *25*), in wild-type FucA with a cobalt instead of the zinc ion (green) (*25*), in mutant Y113F (orange), in mutant R212A (yellow), and in mutant T26A (red). Proposed interactions of a bound Fuc1P molecule with Glu73, Tyr113′, and Zn^{2+} as well as suggested positions of Tyr209′ and Glu214′ during catalysis are shown in pink. The Zn^{2+} coordination sphere corresponds to that of wild-type FucA ligated with PGH (*26*).

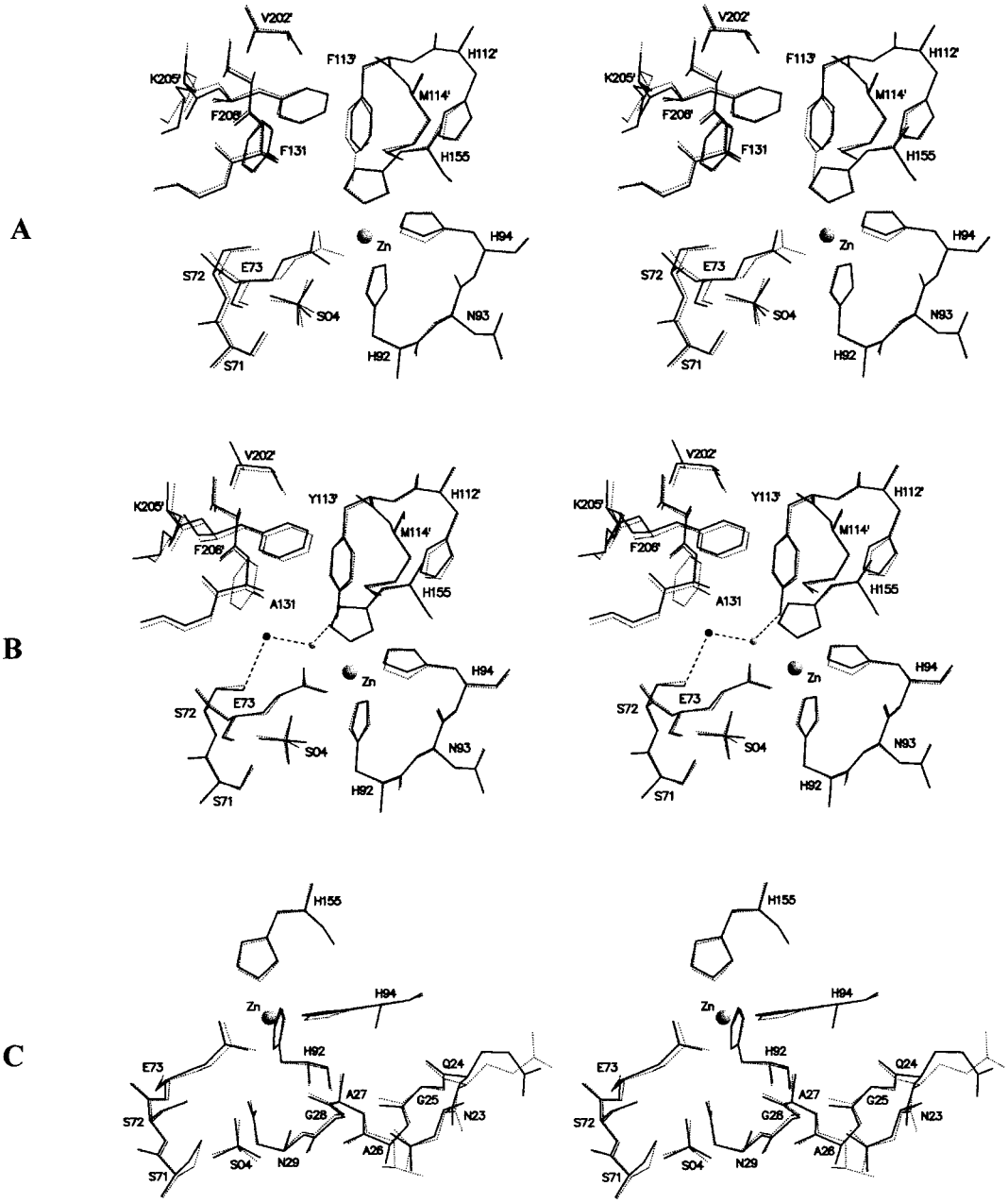

FIGURE 6: Active center of FucA mutant structures (solid line) superimposed with the unligated wild-type structure (dotted line): (A) mutant Y113F, (B) mutant F131A, and (C) mutant T26A. A water molecule near the mutation site in F131A is shown as a small black sphere; it is not present in the wild-type structure. The other water (gray circle) is also observed in the unligated and the PGH-ligated enzyme; it is close to the aldehyde carbonyl oxygen in our model (Figure 8).

exchanging the zinc for a cobalt ion (*25*). In both structures, the side chain of Tyr209′ points away from the active center as it binds to a sulfate at a crystal contact. We assume that this conformation is a packing artifact and that Tyr209′ is mobile enough to reach the catalytic center as indicated by the kinetic data (see below). The conformationally defined parts of the active centers in the three structures with C-terminal mutants were identical to those of the wild type.

In mutants Y113F and Y113F/Y209F, the active center remained intact (Figure 6A). Phe113′ occupied nearly the same position as Tyr113′ in wild-type FucA, but the aromatic ring is further displaced from the zinc coordination sphere as caused by an 11° rotation in χ_1.

In the structure of mutant F131A, the nonpolar wall is changed into a nonpolar pocket because the benzene moiety is missing. The positions of the neighboring side chains of Tyr113′, Lys205′, and Phe206′ are not affected (Figure 6B). Yet, the missing benzene causes higher *B*-factors at the C-terminal end of the structured chain at residues Lys205′ and Phe206′. Furthermore, there is a fixed water molecule at the entrance of this nonpolar pocket, which may explain the reduced activity of this mutant (see below).

The effect of the replacement of Thr26 with Ala is shown in Figure 6C. Loop(23−27) adopts approximately the same conformation as in unligated wild-type FucA, but its flexibility is appreciably reduced (lower *B*-factors). Although loop(23−27) is involved in close intersubunit contacts, the T26A mutation does not disturb the adjacent subunit.

Kinetics of Fuc1P Cleavage. The kinetic data of the various FucA mutants are listed in Table 3. As can be

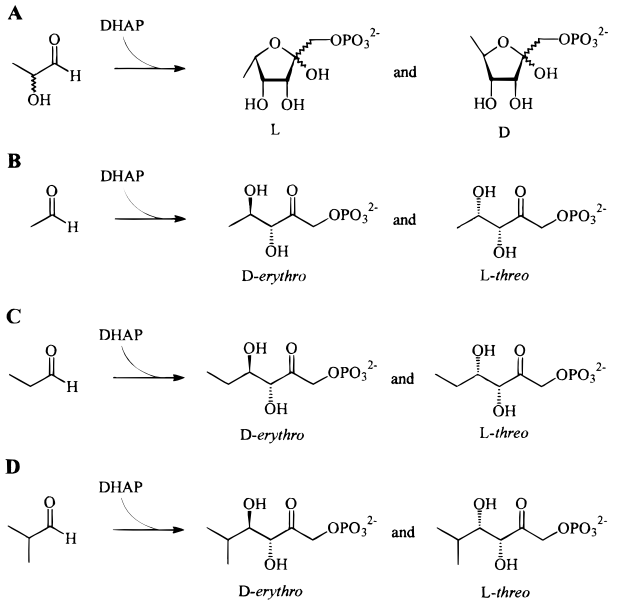

FIGURE 7: Observed products in the aldol addition reaction using FucA mutants with DHAP and different aldehydes (Table 4): (A) *rac*-lactaldehyde, (B) acetaldehyde, (C) propionaldehyde, and (D) isobutyraldehyde.

Table 3: Kinetics for the Cleavage of Fuc1P by FucA Mutants

	relative specific activity[a] (%)	k_{cat}[b] (s^{-1})	K_M (mM)
wild type	100	19.3 (2)	2.2 (0.2)
T26A	14	4.0 (0.3)	6 (0.4)
E73S	0[c]	–	–
Y113F	4.3[d]	0.4 (0.15)	0.5 (0.3)
Y113F/Y209F	0.2[d]	–	–
F131A	0.6	0.6 (0.1)	22 (4)
F131A/F206W	0.1	–	–
F206W	16	8.3 (0.8)	11 (1.0)
Del(207−215)	0.5	1.5 (0.3)	87 (14)
Del(211−215)	7	7.0 (1.0)	21 (3)
K207A	62	19.5 (1.5)	7 (0.5)
Y209F	5[d]	1.3 (0.1)	4.4 (0.6)
R212A	86	12.0 (1.3)	1.8 (0.2)
E214D	95	19.5 (1.0)	3.0 (0.2)
E214Q	71	20.5 (1.0)	6 (0.3)
E214A	48	18.5 (3)	8 (1.3)
E214L	6	12.8 (5)	74 (30)
E215A	90	21.5 (3)	3.1 (0.4)

[a] As measured with 2.4 mM Fuc1P at pH 7.5 and 37 °C. The specific activity of wild-type FucA is 21 units/mg. The chosen Fuc1P concentration followed historical lines. For the wild-type enzyme and for most mutants, it is in the range of or below K_M such that the activity is not at its maximum. The saturation activities can be calculated wherever the k_{cat} and K_M values are given. The error estimates for k_{cat} and K_M are given in parentheses. [b] Referring to one subunit. [c] Detection limit of 0.001%. [d] The enzyme was slowly inactivated, and the data were measured within the first minute.

expected from the structure (*26*), the replacement of Glu73 results in an inactive mutant, here E73S, which confirms that Glu73 is most important for catalysis. Furthermore, it is consistent with the suggestion that Glu73 acts as a catalytic base in the synthetic direction (Figure 3). As for the proposed catalytic acid Tyr113′, the situation is more complicated. The pK_a of a tyrosine is usually above 10 and therefore too high. In our previous work (*26*, *30*), we assumed that the pK_a value of Tyr113′ is considerably lowered by the adjacent Zn^{2+} ion. Now we recognize that mutant Y113F still has an activity of 4.3% of the wild-type value, which is not compatible with the tyrosine acting as the catalytic acid. We therefore modify our view on the enzymatic mechanism and now suggest that the catalytic acid is Glu73 which becomes protonated upon DHAP activation. Glu73 can reach the carbonyl oxygen of the aldehyde (see Figure 8A below).

It should be mentioned that mutant Y113F, like mutant Y209F and the respective double mutant, is slowly inactivated during the enzymatic assay. Both mutations give rise to 20-fold activity reductions. Replacing both tyrosines in mutant Y113F/Y209F caused a 500-fold activity loss; i.e., the effects are multiplicative. Altogether, these data suggest that Tyr113′ is not more essential than Tyr209′ which requires an induced fit to reach the active center. The geometry around Glu73, Tyr113′, and ligated PGH is very tight. After the induced fit upon substrate binding, the hydroxyl of Tyr209′ can reach the carbonyl group of the aldehyde but not Tyr113′. Moreover, there is definitely no space for a water between these tyrosines. We therefore conclude that these two tyrosines function as independent dipoles which assist in carbonyl binding and in stabilizing transition states along the aldol reaction coordinate. This view is supported by the fact that both mutants decrease k_{cat} rather than increase K_M.

An overview of the mutations in the mobile C-terminal tail is given in Figure 4. Mutant Del(207−215) lacking the complete tail had only 0.5% of the wild-type activity, demonstrating that this tail is actually involved in the catalysis as already discussed with mutant Y209F. Interestingly, the very end of the chain is not as important as residues 207−210, because mutant Del(211−215) exhibits an intermediate level of activity. Further mutations in the tail elucidated the roles of some ot its residues.

No significant effect was observed after replacing Arg212′ and Glu215′. Exchanging Glu214′, however, resulted in an activity loss along the series Glu → Asp → Gln → Ala → Leu, which is mainly due to an increase in K_M (2.2 → 3 → 6 → 8 → 74 mM). This is a strong indication that Glu214′ is directly involved in substrate binding. In our model for the induced fit of the mobile C-terminal tail in Figure 5, we suggest that Glu214′ binds to Thr26 and to Tyr209′, which is thereby stabilized.

A similar effect was observed for mutant K207A with a K_M of 7 mM. From the X-ray structure of wild-type FucA, however, it is unlikely that the Lys207′ amino group may directly interact with the substrate during catalysis as it pointed to the solvent in those cases where we observed a defined conformation (Figure 5). Therefore, an indirect participation of Lys207′ seems more plausible, e.g., by remaining in the entropically favorable solvent environment and thus promoting the correct induced fit conformation of the C-terminal tail. The strongest effect among the tail residues was observed for mutant Y209F as described above.

To summarize, the kinetic data suggest that the mobile C-terminal tail undergoes an induced fit, after which it covers the active center and promotes the catalysis. A mobile C-terminus containing a catalytically competent tyrosine had also been observed with class I aldolases (*12*), where this tyrosine is highly conserved and was suggested to facilitate H^+ transfer. A Tyr → Ser replacement in the human class I fructose 1,6-bisphosphate aldolase caused a 16-fold decrease in k_{cat} for isozyme A, but no change in isozyme B (*47*).

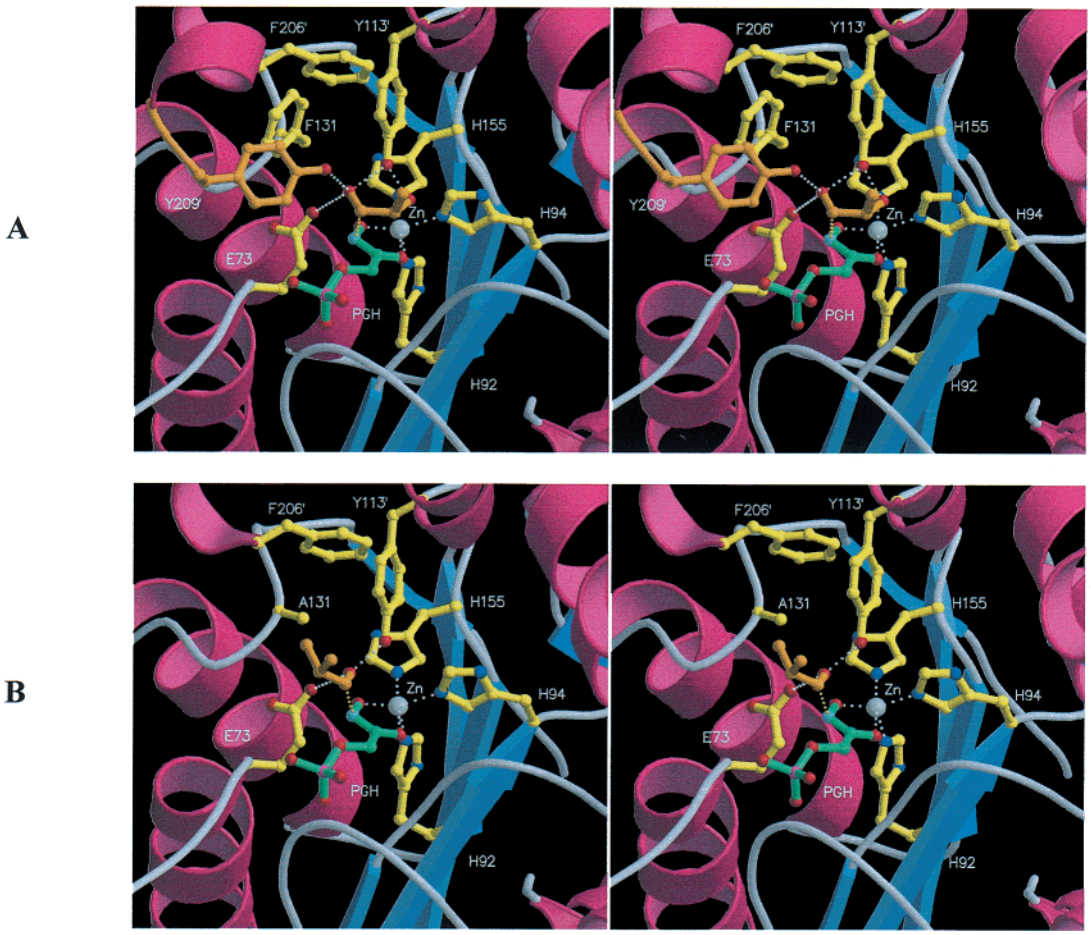

FIGURE 8: Aldehyde binding models indicating the possible involvement of the mobile C-terminal tail via Tyr209′ (orange): (A) L-lactaldehyde (orange) as bound to wild-type FucA and (B) isobutyraldehyde (orange) as bound to mutant F131A yielding exclusively the L-*threo* diastereomer (Table 4). Modeling was carried out manually on the basis of the structures of mutant F131A and of wild-type FucA (*26*).

The activity of FucA is very sensitive to mutations within the nonpolar wall (Figure 2A). A drastic decrease was observed for mutant F131A which exhibited only 0.6% of wild-type activity; the structure is shown in Figure 6B. Here we observed a fixed water molecule at the entrance of the pocket produced by the exchange, which interferes with substrate binding and thus hampers catalysis. A smaller effect was found with mutant F206W in which this nonpolar wall is enlarged. F206W had 16% of the wild-type activity; the drop was mostly caused by an increase in K_M. The corresponding double mutant F131A/F206W had an even lower activity than the two single mutants. The effects were multiplicative like those of the other double mutant (Table 3).

When Thr26, which exhibited the largest displacement upon PGH binding, was replaced by Ala, the activity decreased by a factor of 7, mostly in k_{cat}. The effect is too small to attribute a major catalytic role to Thr26. We suggest that it binds Glu214′ after the induced fit (Figure 5). Moreover, Thr26 is likely to facilitate a relative movement between subunits that may be required for catalysis.

Selectivity of Wild-Type FucA. The selectivity data for reactions in the synthetic direction are given in Table 4. It had been shown that FucA is highly selective with respect to DHAP (*48*), but accepts a wide variety of aldehyde compounds (*2*, *3*, *6*, *49*). For certain types of aldehydes, the L-*threo* diastereomer is observed alongside the expected D-*erythro* product (Figure 7). These diastereomers are consistent with an ordered mechanism, in which DHAP binds first with its carbanion *Si* face covered by the polypeptide, and the aldehyde binds thereafter. If the aldehyde presents its *Si* or *Re* face to the attacking carbanion (Figure 3), the condensation reaction results in the D-*erythro* or L-*threo* diastereomers, respectively. Different ratios are found when either nonpolar or sterically demanding aldehydes, or those lacking a hydrogen-bonding substituent at the C_α- or C_β-position, are used (*3*, *6*, *9*). Aldehydes with an α-hydroxyl group yield exclusively the D-*erythro* product (*3*, *6*, *49*). Moreover, there is a strong preference for L-configurated α-hydroxy aldehydes (*44*, *49*); wild-type FucA selects the L-enantiomer under kinetically controlled reaction conditions from *rac*-lactaldehyde (Table 4).

Selectivity of FucA Mutants. Some of the mutants are less discriminating than wild-type FucA and accept D-lactaldehyde to a larger extent. For mutant Y113F, for instance, the enantioselectivity is almost inverted (Table 4). Mutant Del-(207−215) lacking the complete C-terminal tail and mutant F131A show slight preferences for the D-aldehyde. Mutant Y209F does not discriminate between the enantiomers. All other mutants prefer the L-aldehyde, although the preference is less pronounced than in the wild type.

Similar effects were observed with respect to the diastereoselectivity for the addition of DHAP to the three compounds acet-, propion-, and isobutyraldehyde. Unfortu-

Table 4: Selectivity of FucA Mutants for Different Aldehydes

	rac-lactaldehyde[a] L:D[b]	acetaldehyde[a] D-*erythro*:L-*threo*[b]	propionaldehyde[a] D-*erythro*:L-*threo*[b]	isobutyraldehyde[a] D-*erythro*:L-*threo*[b]
wild type	97:3	95:5	50:50	68:32
T26A	85:15	75:25	–	–
Y113F	10:90[c]	35:65	–	–
F131A	32:68[d]	30:70	3:97	3:97
F206W	70:30	50:50	36:64	60:40
Del(207−215)	40:60[c]	65:35	–	–
Del(211−215)	80:20	54:46	–	–
Y209F	50:50	35:65	–	–
R212A	95:5	95:5	–	–
E214A	71:29	86:14	60:40	75:25
E214L	89:11	70:30	58:42	48:52
E215A	90:10	85:15	–	–

[a] Aldehyde compounds used in FucA-catalyzed aldol condensation using DHAP as the donor. [b] Ratio of observed products as specified in Figure 7. [c] The ^{1}H NMR analysis could not distinguish between the expected D-*erythro* (Figure 7) and a possible L-*threo* product. [d] The ^{1}H NMR data indicate the D-*erythro* product.

nately, not all of the mutants could be examined because some activities, especially with the larger aldehydes, were rather low. Wild-type FucA yields mainly the D-*erythro* product for acetaldehyde, but equal amounts of L-*threo* and D-*erythro* products for propionaldehyde, and an excess of the D-*erythro* product for the sterically more demanding isobutyraldehyde (*3*). For acetaldehyde, the three mutants Y113F, F131A, and Y209F showed an inversion of the diastereoselectivity, while all other mutants favored more or less the usual D-*erythro* product. The change was drastic for propion- and isobutyraldehyde processed by mutant F131A, which yielded exclusively the L-*threo* product.

The available selectivity data reveal three prominent residues (Tyr113′, Phe131, and Tyr209′) that are directly involved in positioning the aldehyde component. On the basis of these data and using the PGH-ligated structure of wild-type FucA, we have developed a model for the stereochemically and stereoelectronically correct binding of L-lactaldehyde, which is depicted in Figure 8A. It assumes (i) the nearly coplanar alignment of the DHAP ene-diolate and the carbonyl group of L-lactaldehyde and hydrogen bonds between Tyr113′ and the carbonyl as well as the hydroxyl groups of the aldehyde, (ii) the proximity of the C-3 atom of DHAP and the C-1 atom of lactaldehyde allowing for C−C bond formation, and (iii) the orientation of the aldehyde with its *Si* face pointing to the C-3 atom of DHAP, which results in the naturally observed D-*erythro* diastereomer. This interpretation was supported by modeling possible transition states using energy-minimized docking with the program SCULPT (*50*) and PGH-ligated FucA.

This model explains why wild-type FucA processes α-hydroxy aldehydes to D-*erythro* diastereomers, as this hydroxyl interacts with Tyr113′ and probably also weakly with Zn^{2+}. For FucA mutants, the reaction geometry is disturbed such that the α-hydroxy of D-lactaldehyde may bind to Tyr113′ as well, reducing the enantioselectivity. This perturbation also occurs with mutants in the mobile C-terminal tail because these do change the enantioselectivity, too (Table 4).

Mutant F131A is rather spectacular because it causes an unexpectedly sharp activity decrease, reverses the enantioselectivity for lactaldehyde, and completely reverses the diastereoselectivity for larger nonpolar aldehydes. Among these observations, the production of the L-*threo* diastereomers can be well understood from the F131A structure; the nonpolar wall at the active center had become a nonpolar pocket, which provides enough space for the aliphatic moiety of the aldehyde such that it favors an aldehyde orientation where the *Re* face can be attacked by the carbanion, as depicted, for example, in Figure 8B.

Conclusion. We have explored the active center of FucA with a number of mutations and by analyzing the structural and catalytical consequences of these changes. The results show that the mobile C-terminal tail performs an induced fit upon substrate binding and that two of its residues contribute directly to the catalysis. Moreover, they led to a modification of the proposed reaction mechanism as noted in the legend of Figure 3. We now propose that Glu73 acts as a base *and* as an acid during catalysis. In the unligated enzyme, Glu73 binds to Zn^{2+} and is deprotonated. When DHAP or Fuc1P binds, it is pushed aside into a nonpolar environment where its pK_a increases such that it can easily deprotonate either the C-3 atom of DHAP or the O-4 atom of Fuc1P, delivering the proton to the other side of the formed or broken C−C bond, respectively. The data further demonstrate the importance of the immediate environment of Glu73, as removal of the adjacent nonpolar wall in F131A changes the selectivities dramatically.

ACKNOWLEDGMENT

We thank C. Müller-Dieckmann for measurements.

REFERENCES

1. Ghalambor, M. A., and Heath, E. C. (1962) *J. Biol. Chem. 237*, 2427−2433.
2. Ozaki, A., Toone, E. J., Von der Osten, C. H., Sinskey, A. J., and Whitesides, G. M. (1990) *J. Am. Chem. Soc. 112*, 4970−4971.
3. Fessner, W.-D., Sinerius, G., Schneider, A., Dreyer, M., Schulz, G. E., Badia, J., and Aguilar, J. (1991) *Angew. Chem., Int. Ed. Engl. 30*, 555−558.
4. Whitesides, G. M., and Wong, C.-H. (1985) *Angew. Chem., Int. Ed. Engl. 24*, 617−638.
5. Bednarski, M. D., Simon, E. S., Bischofberger, N., Fessner, W.-D., Kim, M.-J., Lees, W., Saito, T., Waldmann, H., and Whitesides, G. M. (1989) *J. Am. Chem. Soc. 111*, 627−635.
6. Fessner, W.-D., and Walter, C. (1996) *Top. Curr. Chem. 184*, 97−194.
7. Petersen, M., Zannetti, M. T., and Fessner, W.-D. (1997) *Top. Curr. Chem. 186*, 87−117.
8. Wong, C.-H., Halcomb, R. H., Ichikawa, Y., and Kajimoto, T. (1995) *Angew. Chem., Int. Ed. Engl. 34*, 412−432.

9. Fessner, W.-D. (1995) in *Houben-Weyl Methods of Organic Chemistry* (Helmchen, G., Hoffmann, R. W., Mulzer, J., and Schaumann, E., Eds.) Vol. E21b, pp 1736−1747, Thieme-Verlag, Stuttgart, Germany.
10. Horecker, B. L., Tsolas, O., and Lai, C. Y. (1972) in *The Enzymes* (Boyer, P. D., Ed.) 3rd ed., Vol. 7, pp 213−258, Academic Press, New York.
11. Gefflaut, T., Blonski, C., Perie, J., and Willson, M. (1995) *Prog. Biophys. Mol. Biol. 63*, 301−340.
12. Littlechild, J. A., and Watson, H. C. (1993) *Trends Biochem. Sci. 18*, 36−39.
13. Jia, J., Schörken, U., Lindqvist, Y., Sprenger, G. A., and Schneider, G. (1997) *Protein Sci. 6*, 119−224.
14. Sygusch, J., Beaudry, D., and Allaire, M. (1987) *Proc. Natl. Acad. Sci. U.S.A. 84*, 7846−7850.
15. Blom, N., and Sygusch, J. (1997) *Nat. Struct. Biol. 4*, 36−39.
16. Gamblin, S. J., Davies, G. J., Grimes, J. M., Jackson, R. M., Littlechild, J. A., and Watson, H. C. (1991) *J. Mol. Biol. 219*, 573−576.
17. Dalby, A., Dauter, Z., and Littlechild, J. A. (1999) *Protein Sci. 8*, 291−297.
18. Hester, G., Brenner-Holzach, O., Rossi, F. A., Struck-Donatz, M., Winterhalter, K. H., Smit, J. D. G., and Piontek, K. (1991) *FEBS Lett. 292*, 237−242.
19. Kim, H., Certa, U., Döbeli, H., Jakob, P., and Hol, W. G. J. (1998) *Biochemistry 37*, 4388−4396.
20. Mavridis, I. M., Hatada, M. H., Tulinsky, A., and Lebioda, L. (1982) *J. Mol. Biol. 162*, 419−444.
21. Izard, T., Lawrence, M. C., Malby, R., Lilley, G. G., and Colman, P. M. (1994) *Structure 2*, 361−369.
22. Lawrence, M. C., Barbosa, J. A. R. G., Smith, B. J., Hall, N. E., Pilling, P. A., Ooi, H. C., and Marcuccio, S. M. (1997) *J. Mol. Biol. 266*, 381−399.
23. Hennig, M., D'Arcy, A., Hampele, I. C., Page, M. G. P., Oefner, C., and Dale, G. E. (1998) *Nat. Struct. Biol. 5*, 357−362.
24. Dreyer, M. K., and Schulz, G. E. (1993) *J. Mol. Biol. 231*, 549−553.
25. Dreyer, M. K., and Schulz, G. E. (1996) *Acta Crystallogr., Sect. D 52*, 1082−1091.
26. Dreyer, M. K., and Schulz, G. E. (1996) *J. Mol. Biol. 259*, 458−466.
27. Blom, N. S., Tétreault, S., Coulombe, R., and Sygusch, J. (1996) *Nat. Struct. Biol. 3*, 856−862.
28. Cooper, S. J., Leonard, G. A., McSweeney, S. M., Thompson, A. W., Naismith, J. H., Qamar, S., Plater, A., Berry, A., and Hunter, W. N. (1996) *Structure 4*, 1303−1315.
29. Hall, D. R., Leonard, G. A., Reed, C. D., Watt, C. I., Berry, A., and Hunter, W. N. (1999) *J. Mol. Biol. 287*, 383−394.
30. Fessner, W.-D., Schneider, A., Held, H., Sinerius, G., Walter, C., Hixon, M., and Schloss, J. V. (1996*) Angew. Chem., Int. Ed. Engl. 35*, 2219−2221.
31. Johnson, A. E., and Tanner, M. E. (1998) *Biochemistry 37*, 5746−5754.
32. Kunkel, T. A., Roberts, J. D., and Zakour, R. A. (1987) *Methods Enzymol. 154*, 367−382.
33. Taylor, J. W., Ott, J., and Eckstein, F. (1985) *Nucleic Acids Res. 13*, 8765−8785.
34. Gill, S. C., and Hippel, P. H. (1989) *Anal. Biochem. 182*, 319−326.
35. Schulz, G. E., Dreyer, M., Klein, C., Kreusch, A., Mittl, P., Müller, C. W., Müller-Dieckmann, J., Muller, Y. A., Proba, K., Schlauderer, G., Spürgin, P., Stehle, T., and Weiss, M. S. (1992) *J. Cryst. Growth 122*, 385−392.
36. Kabsch, W. (1988) *J. Appl. Crystallogr. 21*, 916−924.
37. Brünger, A. T. (1992) *X-PLOR Manual Version 3.0*, Yale University, New Haven, CT.
38. Murshudov, G. N., Vagin, A. A., and Dodson, E. J. (1997) *Acta Crystallogr., Sect. D 53*, 240−255.
39. Lamzin, V. S., and Wilson, K. S. (1993) *Acta Crystallogr., Sect. D 49*, 129−147.
40. Jones, T. A., Zou, J.-Y., Cowan, S. W., and Kjeldgaard, M. (1991) *Acta Crystallogr., Sect. A 47*, 110−119.
41. Kraulis, P. J. (1991) *J. Appl. Crystallogr. 24*, 946−950.
42. Merritt, E. A., and Bacon, D. J. (1997) *Methods Enzymol. 277*, 505−524.
43. Ghalambor, M. A., and Heath, E. C. (1966) *Methods Enzymol. 9*, 538−542.
44. Fessner, W.-D., Schneider, A., Eyrisch, O., Sinerius, G., and Badia, J. (1993) *Tetrahedron: Asymmetry 4*, 1183−1192.
45. Fessner, W.-D., and Sinerius, G. (1994) *Angew. Chem., Int. Ed. Engl. 33*, 209−212.
46. Kimura, E., Gotoh, T., Koike, T., and Shiro, M. (1999) *J. Am. Chem. Soc. 121*, 1267−1274.
47. Takahashi, I., Takasaki, Y., and Hori, K. (1989) *J. Biochem. 105*, 281−286.
48. Arth, H.-L., and Fessner, W.-D. (1998) *Carbohydr. Res. 305*, 313−321.
49. Fessner, W.-D., Badia, J., Eyrisch, O., Schneider, A., and Sinerius, G. (1992) *Tetrahedron Lett. 33*, 5231−5234.
50. Surles, M. C., Richardson, J. S., Richardson, D. C., and Brooks, F. P. (1994) *Protein Sci. 3*, 198−210.

BI9927686